Identification and Conformational Study of Stable Radiation-Induced Defects in Sucrose Single Crystals using Density Functional Theory Calculations of Electron Magnetic Resonance Parameters

H. De Cooman,[†,‡] E. Pauwels,[‡] H. Vrielinck,[†] E. Sagstuen,[§] F. Callens,[†] and M. Waroquier*[,‡]

Department of Solid State Sciences, Ghent University, Krijgslaan 281-S1, B-9000 Gent, Belgium, Center for Molecular Modeling, Ghent University, Proeftuinstraat 86, B-9000 Gent, Belgium, and Department of Physics, University of Oslo, P.O. Box 1048 Blindern, N-0316 Oslo, Norway

Received: December 21, 2007

One of the major stable radiation-induced radicals in sucrose single crystals (radical T2) has been identified by means of density functional theory (DFT) calculations of electron magnetic resonance parameters. The radical is formed by a net glycosidic bond cleavage, giving rise to a glucose-centered radical with the major part of the spin density residing at the C_1 carbon atom. A concerted formation of a carbonyl group at the C_2 carbon accounts for the relatively small spin density at C_1 and the enhanced g factor anisotropy of the radical, both well-known properties of this radical from several previous experimental investigations. The experimentally determined and DFT calculated proton hyperfine coupling tensors agree very well on all accounts. The influence of the exact geometrical configuration of the radical and its environment on the tensors is explored in an attempt to explain the occurrence and characteristics of radical T3, another major species that is most likely another conformation of T2. No definitive conclusions with regard to the actual structure of T3 could be arrived at from this study. However, the results indicate that, most likely, T3 is identical in chemical structure to T2 and that changes in the orientation of neighboring hydroxy groups or changes in the configuration of the neighboring fructose ring can probably not account for the type and size of the discrepancies between T2 and T3.

1. Introduction

Considerable efforts were made during the last few decades to gain insight into the radiation chemistry of saccharides. These experimental studies typically rely on electron magnetic resonance (EMR) techniques, such as electron paramagnetic resonance (EPR), electron−nuclear double resonance (ENDOR), and ENDOR-induced EPR (EIE). They have been quite successful in identifying radiation-induced radicals and suggest that some common mechanisms are operative with respect to their formation (rhamnose,[1–6] glucose-1-phosphate,[7] methyl-α-D-glucopyranoside,[8] α-D-glucopyranoside,[9] β-D-fructose,[10] trehalose,[11–13] sucrose[13–19]). However, both identifying radical structures and unraveling their formation mechanisms are still far from trivial tasks, and particularly with regard to radicals stable at room temperature (RT), these studies often have been less conclusive.

In sucrose, trapped electrons[17] and alkoxy radical formation[15] have been reported after irradiation at 4 K. Until recently, however, the experimental studies on stable RT radicals in sucrose single crystals[13,16,18,19] were in disagreement on several points, impeding any attempt at identifying the radical structures and their formation mechanisms. In a recent study,[20] this matter was cleared up, and unambiguous data are now available. In summary, three different radicals, labeled T1, T2, and T3, were spectroscopically characterized, with T2 and T3 being very similar. Furthermore, density functional theory (DFT) calculations presented in that study[20] convincingly showed that the so far most attractive radical model for the T2/T3 radicals proposed in literature[16] was incapable of properly reproducing the experimental data.

A number of semiempirical rules and relations, for example, the McConnell relation[21] and the Heller−McConnell relation,[22] can be used to interpret experimental data in terms of possible radical models. However, if complex molecular changes occur, more general and more powerful tools are necessary. As illustrated in, for example, refs 23–27, DFT based quantum chemical calculations have proven to be particularly useful for assisting in structure assignments: comparison of experimentally obtained EMR results with parameters calculated for a certain radical structure using DFT may provide arguments for either rejection or validation of a proposed radical model. However, DFT calculations are not capable of predicting which radicals will be formed, and often a large number of radical models can be devised that potentially could account for a certain set of experimental results. For carbohydrates, this problem is pronounced, as there are no characteristic functional groups distinguishing between possible radical sites and there are no characteristic magnetic nuclei distinguishing between possible radical models. In this context, the semiempirical rules provide valuable information to discriminate between different radical models. For the limited list of plausible radical candidates thus obtained, DFT calculations can be employed in order to identify the actual radical structure. The current work provides an excellent illustration of this synergy: a set of possible radical models is inferred from the experimental data, and DFT calculations are subsequently employed to positively identify one of these as the proper structure of the T2 radical. Furthermore, the sensitivity of the calculated hyperfine (HF)

* To whom all correspondence should be addressed. Phone: 003292646559. Fax: 003292646697 . E-mail: michel.waroquier@ugent.be.
† Department of Solid State Sciences, Ghent University.
‡ Center for Molecular Modeling, Ghent University.
§ Department of Physics, University of Oslo.

10.1021/jp712004g CCC: $40.75 © 2008 American Chemical Society
Published on Web 05/29/2008

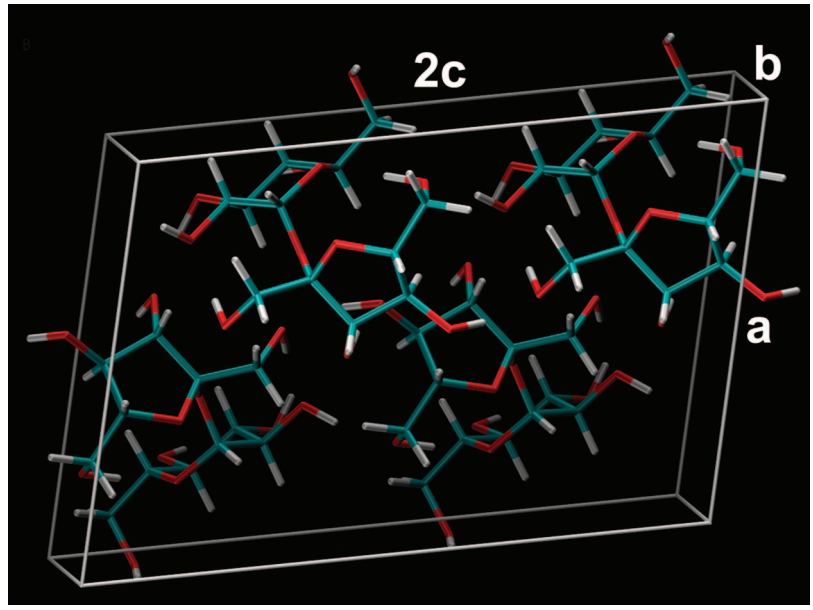

Figure 1. Three-dimensional structure of the <ab2c> supercell used for periodic geometry optimizations in the current work, obtained by doubling the crystal unit cell in the <c> direction. The atomic coordinates were taken from ref 50.

coupling tensors to the precise conformation of the radical and its environment is explored in an attempt to understand the coexistence and the characteristics of the T3 radical.

2. Computational Procedures

2.1. Geometry Optimizations. The stable geometry of a given molecular radical species obviously depends on the actual environment. In sugar single crystals, this environment consists of a periodic lattice, primarily governed by inter- and intramolecular hydrogen bonds. When the radical model is expected to involve considerable nuclear and electronic reorganization, geometry optimizations should be performed using a theoretical methodology that appropriately accounts for this environment. In the literature, both cluster[24,25] and periodic[28] approaches have proven successful in modeling free radical structures in the solid state. As a periodic model exploits the translational symmetry of the crystal, it automatically and fully incorporates the full lattice environment and therefore offers the most complete description of a crystalline system. This approach does not require the artificial constraints that have to be imposed on the boundary molecules/atoms within a cluster methodology. Because the number of atoms can be substantially decreased as compared with a typical, physically sound cluster, the computational cost can also be considerably reduced. Moreover, a very recent study by Declerck and co-workers on sugar radicals[29] has shown that (i) the accuracy of the calculated EMR parameters depends chiefly on the accuracy of the geometry and (ii) that this geometry is most accurately predicted within a periodic model. Therefore, a periodic approach was adopted in the present work for all geometry optimizations. To ensure that the radical was well-separated from its periodic images, an <ab2c> supercell (180 atoms) was used, obtained by doubling the original crystal unit cell in the <c> direction. This supercell is depicted in Figure 1. To corroborate the validity of this model, a reference calculation was performed with the considerably larger and therefore computationally much more demanding <2a2b2c> supercell (720 atoms). All calculations were performed with the CPMD software package,[30] using a BP86 gradient-corrected density functional,[31,32] together with a plane wave basis set (with a maximum kinetic energy of 25 Ry for the plane waves) and ultrasoft pseudopotentials of the Vanderbilt type.[33] Unless explicitly mentioned, no constraints were imposed on the atoms of the supercell.

2.2. Calculation of EMR Parameters. Within the CPMD software package, pseudopotentials are employed in the calculation of EMR parameters. This method is known to reproduce less accurately the HF coupling tensors, in particular, the isotropic values, as compared with an all electron approach.[34] On the other hand, several studies, for example, refs 29 and 35, have clearly shown that incorporation of the molecular environment can have an appreciable effect on the calculated EMR parameters. Therefore, the same hybrid periodic/cluster model used in our previous work[20] was adopted: HF coupling tensors were calculated using the Gaussian03 software suite[36] on a cluster that was cut out of each periodically optimized structure such that it contained the radical and all (intact) molecules hydrogen bound to it (10 surrounding sucrose molecules in total). The B3LYP functional[37] and a 6−311G(d,p) basis set[38,39] were used for all atoms within the cluster. This hybrid model provides highly accurate EMR parameters at a reasonable computational cost.

The cluster approach applied for the calculation of the HF parameters would be computationally too demanding in the case of the g tensor. Therefore, g tensor calculations were performed, also using the Gaussian03 software suite, but only on the optimized radical molecule cut out of the periodically optimized <ab2c> supercell (referred to as Approach #1). Because the environment is completely neglected in this approach, calculations were also performed using the optimized <ab2c> supercell with the CPMD software package (referred to as Approach #2), even if the pseudopotential model is inherently less accurate, also for the g tensor. The code for these calculations has recently been developed by Declerck and co-workers.[40] A BLYP functional form[41,42] was used, together with a 100 Ry cutoff plane wave basis set and Goedecker type norm-conserving pseudopotentials.[43]

Whenever a comparison is made between experimental eigenvectors on the one hand and crystal directions or calculated eigenvectors on the other hand, allowed symmetry operations

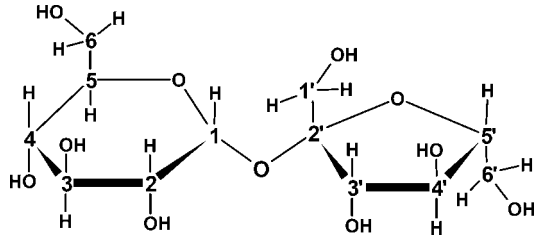

Figure 2. Chemical structure of the sucrose molecule with the atomic numbering used in the present work. Carbon bound hydrogen atoms and oxygen atoms are labeled according to the carbon to which they are bound, and hydroxy protons are labeled according to the oxygen to which they are bound. For example, H_3 is the hydrogen at C_3 and $H(O_3)$ is the hydroxy proton at C_3.

TABLE 1: Proton Hyperfine Coupling Tensors (in MHz) of Stable Radicals T2 and T3 in Room Temperature X-Irradiated Sucrose Single Crystals, Measured at 110 K, Approximately Two Days after Irradiation[a,20]

				eigenvectors			
radical	proton	iso	aniso	a*	b	c	δ (°)
T2	H_α	−38.69	−19.66	0.424	−0.163	−0.891	10.9
			−2.11	0.886	0.280	0.371	14.4
			21.77	0.189	−0.946	0.263	12.1
	$H_{\beta1}$	16.37	−2.32	0.869	−0.355	−0.344	20.9
			−1.72	−0.209	0.368	−0.906	22.4
			4.04	0.448	0.860	0.246	9.8
	$H_{\beta2}$	13.68	−3.09	0.718	−0.650	0.248	14.9
			−2.17	0.638	0.473	−0.608	14.2
			5.26	0.278	0.595	0.754	13.0
T3	H_α	−35.81	−18.98	0.584	−0.184	−0.790	
			−2.11	0.755	0.481	0.446	
			21.09	0.298	−0.857	0.420	
	$H_{\beta1}$	16.42	−2.10	0.840	−0.541	−0.034	
			−1.77	0.178	0.334	−0.926	
			3.87	0.512	0.772	0.377	
	$H_{\beta2}$	12.24	−3.62	0.528	−0.822	0.214	
			−2.12	0.804	0.402	−0.439	
			5.74	0.275	0.403	0.873	

[a] In the right hand column, the deviation δ between the eigenvectors of T2 and T3 are given.

were performed on the experimental eigenvectors in such a way that the best possible agreement is obtained.

3. Results and Discussion

3.1. Interpretation of Experimental Results. Figure 2 shows the chemical structure of the sucrose molecule, with the numbering model used in this work. The experimentally determined tensors for the T2 and T3 radicals present in RT irradiated sucrose single crystals are listed in Table 1, as reported in ref 20. From comparison with ENDOR spectra of deuterated crystals, it was established that all of these interactions arise from nonexchangeable protons.[16,20]

The T2 and T3 radicals are essentially characterized by three proton HF couplings: one larger coupling due to an α-proton interaction and two smaller couplings due to either β- or γ-proton interactions. The spin density on an α proton can be estimated using either the isotropic (McConnell relation,[21] eq 1) or the anisotropic values (Gordy−Bernhard relation,[44] eq 2) of the HF coupling tensor:

$$a^{\alpha}_{\mathrm{iso}} = Q^{\alpha}_{\mathrm{iso}}\rho^{\pi} \quad (1)$$

$$b^{\alpha}_{+,\mathrm{aniso}} = Q^{\alpha}_{\mathrm{aniso}}\rho^{\pi} \quad (2)$$

where $a^{\alpha}_{\mathrm{iso}}$ is the isotropic component, $b^{\alpha}_{+,\mathrm{aniso}}$ is the most positive dipolar component, ρ^{π} is the unpaired spin density localized on the carbon in the $2p_z$ lone electron orbital (LEO), and $Q^{\alpha}_{\mathrm{iso}}$ and $Q^{\alpha}_{\mathrm{aniso}}$ are empirical "constants", dependent to some extent on the nature of the radical fragment. For $Q^{\alpha}_{\mathrm{iso}}$, a value of −72 MHz is generally assumed,[45] and for $Q^{\alpha}_{\mathrm{aniso}}$, a value of 38.7 MHz was proposed.[46] As stated previously,[20] eqs 1 and 2 both yield unpaired spin densities of 0.50−0.55 for both radicals (T2 and T3), indicating that about 50% of the unpaired spin density is delocalized on other nuclei and, furthermore, that the spin centers are essentially planar.[46] Sagstuen et al. made similar observations[16] and suggested the presence of a neighboring carbonyl group as an explanation. This would account for the delocalization and also for the g factor anisotropy being larger than that for a typical carbon-centered radical. This proposal was further corroborated by the results obtained by Flores and co-workers[47] and Yordanov and Karakirova.[48] For X-irradiated sucrose powder and single crystals, these authors found an increase in the intensity of certain bands in the optical absorption spectrum in the UV region, linearly dependent on the applied radiation dose. Some of these absorption bands (λ = 250 and 320 nm) are typically associated with carbonyl groups in organic compounds.

Sagstuen et al. proposed two specific radical models containing a carbonyl group,[16] but it was shown in ref 20 that these could not account for the experimentally observed proton HF couplings. Nevertheless, the compelling evidence for the presence of a neighboring carbonyl group urged us to explore this path further in the present work. A large variety of tentative radical models containing a carbonyl group next to the carbon site of the unpaired spin density can be envisioned, however.

TABLE 2: Comparison of C···H Directions in the Pristine Crystal Molecule (Calculated Using the Atomic Coordinates Reported in Ref 50) with the Directions of the Eigenvectors Corresponding to the Most Positive Anisotropic Hyperfine Coupling Values of $H_{\beta1}$(T2), $H_{\beta2}$(T2), $H_{\beta1}$(T3), and $H_{\beta2}$(T3) (Table 1)[a]

			direction cosines			δ (°)		δ (°)	
	hydrogen position	distance (Å)	a*	b	c	$H_{\beta1}$(T2)	$H_{\beta2}$(T2)	$H_{\beta1}$(T3)	$H_{\beta2}$(T3)
$C_1\cdots H_3$	γ	2.78	0.428	−0.897	−0.112	20.7		29.6	
$C_1\cdots H_5$	γ	2.74	0.138	−0.647	0.750		8.5		17.6
$C_3\cdots H_1$	γ	3.46	−0.150	0.984	0.092	27.0		36.7	
$C_3\cdots H_5$	γ	2.79	−0.082	0.235	−0.968		26.7		15.7
$C_4\cdots H_2$	γ	2.69	−0.148	0.652	−0.744	36.0		30.8	
$C_4\cdots H_5$	β	2.15	0.542	0.443	0.714		17.7		18.0
$C_{3'}\cdots H_{1'a}$	γ	2.74	−0.173	0.534	−0.828		8.1		9.9
$C_{3'}\cdots H_{1'b}$	γ	3.50	−0.568	0.203	−0.797		28.3		20.9
$C_{3'}\cdots H_{5'}$	γ	2.87	−0.515	0.762	0.394	37.9		45.3	

[a] δ denotes the angle between the directions.

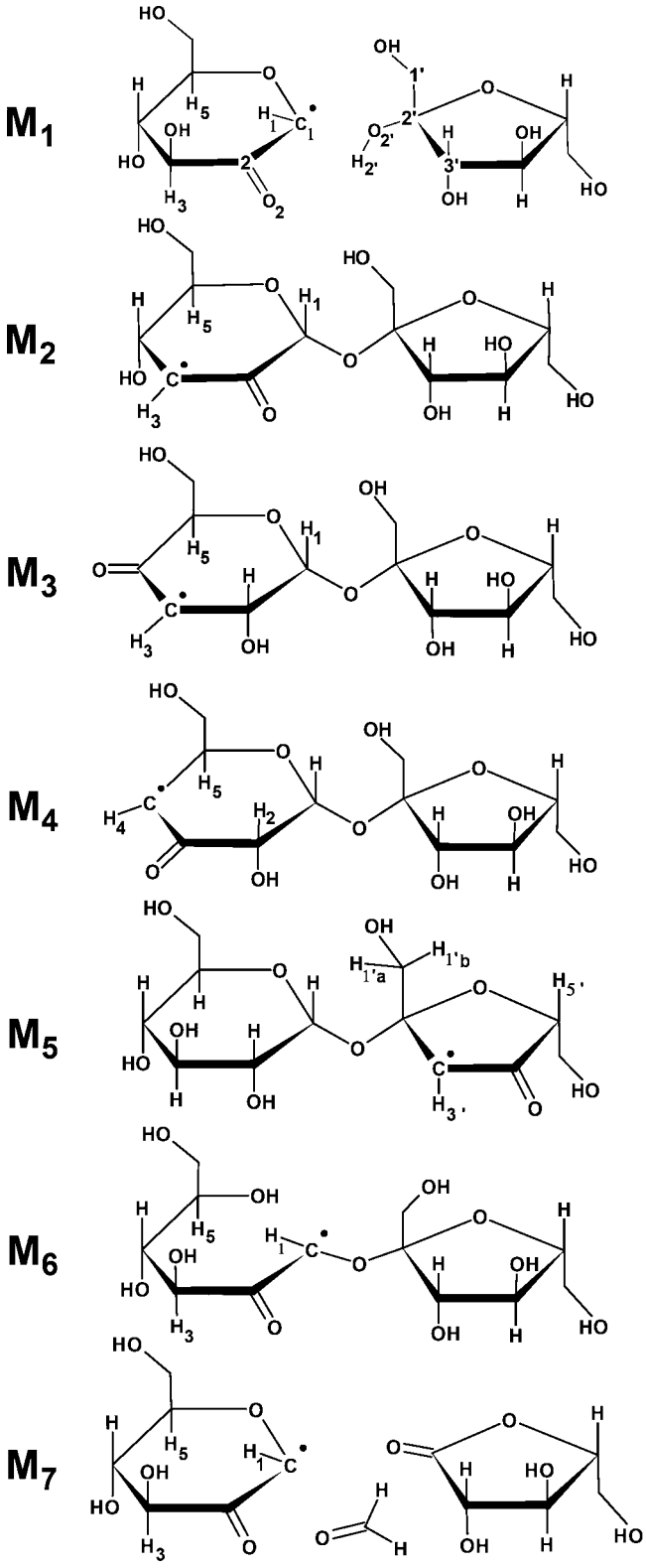

Figure 3. Chemical structure of the different radical models for which DFT geometry optimizations and EMR calculations were performed (see Table 3).

Important additional information can be obtained from the anisotropy of the two smaller HF couplings which is smaller than usual for regular β-type proton HF interactions. Because the experimental $H_{\beta 1}$ and $H_{\beta 2}$ tensors display a typical dipolar anisotropic shape (Table 1), a classical point dipole−dipole approximation is expected to be valid. In this approximation, the most positive dipolar component $b_{+,\mathrm{dip}}$ is dependent on the electron−nucleus distance r as

$$b_{+,\mathrm{dip}} = \frac{\rho^{\pi}\mu_0 g \mu_B g_N \mu_N}{2\pi r^3}$$

where ρ^{π} is the unpaired spin density localized in the LEO, and μ_0, g, μ_B, g_N, and μ_N are the vacuum permeability, the radical g value, the Bohr magneton, the proton nuclear g factor, and the nuclear magneton respectively. Approximating g by the free electron g value of 2.0023 and assuming $\rho_{\pi} = 0.5$ (see above), the values for $b_{+,\mathrm{dip}}$ in Table 1 yield values for r of 2.7 Å and 2.4−2.5 Å for the $H_{\beta 1}$ and $H_{\beta 2}$ protons, respectively. These values are considerably higher than the typical $C_{\alpha}\cdots H_{\beta}$ distance of 2.1 Å in the sucrose molecule. The former value, in particular, more closely resembles the typical $C_{\alpha}\cdots H_{\gamma}$ distance of 2.7−2.8 Å. This suggests that $H_{\beta 1}$ and probably also $H_{\beta 2}$ are actually γ protons. The fact that the isotropic coupling values of about 15 MHz are rather large does not invalidate this hypothesis. Box and co-workers have convincingly argued[49] that the magnitude of the γ-proton isotropic HF couplings is strongly dependent on the exact conformation of the radical. Therefore, tentative models should be considered where $H_{\beta 1}$ and possibly also $H_{\beta 2}$ are in fact γ-protons, rather than β-protons as presumed by Sagstuen et al.

Unless a ring opening event occurs, $C_{\alpha}\cdots H_{\gamma}$ directions and distances are not expected to change much as compared to the values for the pristine crystal molecule because of the relatively large spatial separations. It is well-known that the eigenvector associated with $b_{+,\mathrm{dip}}$ is oriented roughly along the line connecting the (main) site of the unpaired spin with the interacting nucleus. Therefore, a comparison was made between the eigenvectors associated with $b_{+,\mathrm{dip}}$ and the directions of the different $C_{\alpha}\cdots H_{\beta}$ and $C_{\alpha}\cdots H_{\gamma}$ of the pristine crystal. For $H_{\beta 1}$, only hydrogen atoms at a γ-position were considered; for $H_{\beta 2}$, hydrogen atoms at both β- and γ-positions were considered. Also, only carbon bound hydrogen atoms should be considered, since all HF interactions arise from nonexchangeable protons. The directions were calculated from the atomic coordinates reported in ref 50.

For only a few cases, an acceptable agreement was found between the $C_{\alpha}\cdots H_{\beta}$ or $C_{\alpha}\cdots H_{\gamma}$ direction and the two smaller HF interactions. The results are shown in Table 2. The corresponding radical models are depicted in Figure 3 and labeled M_1−M_5. For the C_1 centered radical M_1, a scission of the glycosidic bond is necessary whereas the other models require the net abstraction of a hydroxy group. Ring opening events are not considered: if a hydroxy group would be present at an α position, the hydroxy hydrogen hyperfine coupling should have been detected experimentally. Thus, a limited number of radical models is arrived at and these can now be investigated further by DFT methods.

3.2. Radical Model Assignment. Geometry optimizations and calculations of EMR parameters were performed for radical models M_1 to M_5 (Figure 3) as described in Computational Procedures. In Table 3, the results are reported and compared with the experimental data. For most models, the agreement between calculated and experimental HF tensors is very poor for at least one of the couplings. Apart from other discrepancies, models M_2, M_3, and M_4 may readily be discarded as they would give rise to a β-proton interaction with an isotropic component of more than 100 MHz. Model M_5 can also be dismissed, among others because the directions of the α-proton eigenvectors are off by 50° and more. For model M_1, however, the agreement between the

TABLE 3: Proton Hyperfine Coupling Tensors (in MHz) for Radical Models M_1-M_7, Shown in Figure 3, Obtained by Means of DFT Calculations As Described in Computational Procedures[a]

				eigenvectors				δ (°)	
radical model	proton	iso	aniso	a*	b	c	proton	T2	T3
$\mathbf{M_1}$	$\mathbf{H_1}$	−34.60	−20.23	−0.451	0.155	0.879	$\mathbf{H_\alpha}$	1.8	9.3
			−4.66	0.875	0.267	0.403		2.1	14.3
			24.89	−0.173	0.951	−0.256		1.2	13.0
	$\mathbf{H_3}$	16.18	−2.16	0.874	0.462	0.154	$\mathbf{H_{\beta 1}}$	29.5	11.9
			−1.86	−0.249	0.152	0.957		29.5	11.4
			4.02	−0.418	0.874	−0.248		1.9	10.9
	$\mathbf{H_5}$	12.59	−2.88	0.675	0.673	0.303	$\mathbf{H_{\beta 2}}$	4.2	13.1
			−2.06	0.698	−0.450	−0.557		4.7	9.5
			4.95	0.239	−0.588	0.773		2.5	12.2
$\mathbf{M_2}$	$\mathbf{H_3}$	−42.75	−24.29	0.513	0.635	−0.577	$\mathbf{H_\alpha}$	33.4	29.2
			−3.72	0.836	−0.218	0.503		8.9	16.2
			28.01	−0.194	0.741	0.643		33.6	32.1
	$\mathbf{H_1}$	0.53	−2.38	0.804	−0.071	0.590	$\mathbf{H_{\beta 1}}$	61.9	46.0
			−0.92	0.567	0.390	−0.726		66.7	25.5
			3.30	−0.178	0.918	0.353		38.5	41.4
	$\mathbf{H_5}$	−1.29	−2.96	0.066	0.986	−0.151	$\mathbf{H_{\beta 2}}$	49.4	35.6
			−1.71	0.974	−0.096	−0.204		37.7	24.3
			4.67	0.215	0.134	0.967		44.8	31.8
	$\mathbf{H_4}$	111.31	−5.74	0.167	0.836	0.523			
			−0.91	0.334	−0.547	0.767			
			6.65	0.928	0.046	−0.371			
$\mathbf{M_3}$	$\mathbf{H_3}$	−45.44	−26.53	0.148	0.762	−0.630	$\mathbf{H_\alpha}$	41.6	43.5
			−3.51	0.948	0.073	0.311		20.9	35.0
			30.04	−0.283	0.643	0.711		42.1	40.0
	$\mathbf{H_1}$	−1.05	−2.23	0.796	0.155	−0.585	$\mathbf{H_{\beta 1}}$	18.5	39.4
			−1.47	0.600	−0.070	0.797		34.7	52.6
			3.69	−0.083	0.985	0.148		32.0	41.7
	$\mathbf{H_5}$	−6.20	−2.87	0.880	−0.474	−0.018	$\mathbf{H_{\beta 2}}$	20.6	31.7
			−1.25	0.432	0.817	−0.383		26.6	32.5
			4.11	0.196	0.329	0.924		18.8	6.9
	$\mathbf{H_2}$	114.91	−5.60	0.036	0.357	0.933			
			−1.41	0.881	0.429	−0.199			
			7.01	−0.472	0.829	−0.299			
$\mathbf{M_4}$	$\mathbf{H_4}$	−45.75	−26.21	−0.296	0.267	0.917	$\mathbf{H_\alpha}$	9.6	18.7
			−3.72	0.944	−0.065	0.323		20.3	34.3
			29.93	0.146	0.962	−0.232		19.4	28.5
	$\mathbf{H_2}$	2.25	−2.49	0.864	0.334	0.378	$\mathbf{H_{\beta 1}}$	42.3	26.6
			−1.29	−0.498	0.451	0.741		42.9	22.4
			3.78	−0.077	0.828	−0.556		28.0	27.4
	$\mathbf{H_5}$	106.43	−5.56	0.639	0.626	−0.447	$\mathbf{H_{\beta 2}}$	86.6	74.1
			−1.42	0.729	−0.679	0.090		84.9	74.1
			6.98	0.247	0.383	0.890		14.5	2.2
$\mathbf{M_5}$	$\mathbf{H_{3'}}$	−47.77	−27.86	0.378	0.307	0.873	$\mathbf{H_\alpha}$	48.2	58.3
			−3.75	0.435	0.774	−0.461		64.5	60.3
			31.61	0.817	−0.554	−0.159		50.5	49.4
	$\mathbf{H_{5'}}$	−0.71	−2.30	0.577	0.627	−0.523	$\mathbf{H_{\beta 1}}$	25.3	32.6
			−1.11	0.486	0.251	0.837		17.7	39.4
			3.40	−0.656	0.737	0.160		27.3	32.4
	$\mathbf{H_{1'a}}$	1.89	−4.20	0.725	−0.562	−0.399	$\mathbf{H_{\beta 2}}$	86.8	80.5
			−1.69	0.689	0.575	0.441		84.2	82.6
			5.89	−0.018	−0.595	0.804		17.3	20.5
	$\mathbf{H_{1'b}}$	16.51	−2.12	0.278	0.952	0.127	$\mathbf{H_{\beta 2}}$	31.7	16.9
			−1.09	0.667	−0.097	−0.739		23.0	26.0
			3.21	0.691	−0.290	0.662		30.2	27.8
$\mathbf{M_6}$	$\mathbf{H_1}$	−41.28	−22.43	0.649	0.521	0.554	$\mathbf{H_\alpha}$	72.3	81.1
			−3.48	0.677	−0.062	−0.734		71.9	81.1
			25.90	−0.348	0.851	−0.393		13.0	3.3
	$\mathbf{H_3}$	0.24	−2.70	0.703	−0.099	−0.704	$\mathbf{H_{\beta 1}}$	35.1	55.9
			−2.10	0.659	0.461	0.594		32.3	54.1
			4.80	−0.266	0.882	−0.390		13.4	15.5
	$\mathbf{H_5}$	0.49	−1.36	−0.100	0.853	0.512	$\mathbf{H_{\beta 2}}$	52.4	40.7
			−1.12	0.994	0.063	0.091		56.7	42.8
			2.48	−0.045	−0.518	0.854		20.0	19.6
$\mathbf{M_7}$	$\mathbf{H_1}$	−41.14	−22.64	−0.269	0.172	0.948	$\mathbf{H_\alpha}$	9.5	20.3
			−4.27	0.952	0.199	0.234		9.9	23.3
			26.90	−0.149	0.965	−0.217		3.7	15.8
	$\mathbf{H_3}$	6.48	−2.51	0.854	0.520	−0.020	$\mathbf{H_{\beta 1}}$	21.0	1.6
			−1.52	−0.085	0.178	0.980		20.6	10.9
			4.04	−0.513	0.835	−0.196		4.9	11.0
	$\mathbf{H_5}$	13.05	−2.62	0.858	0.507	0.079	$\mathbf{H_{\beta 2}}$	15.1	27.6
			−2.16	−0.410	0.586	0.698		15.5	29.3
			4.79	0.307	−0.632	0.711		3.7	16.2

[a] The deviation δ between the calculated eigenvectors and the eigenvectors of T2 and T3 (Table 1) are given in the right-hand columns.

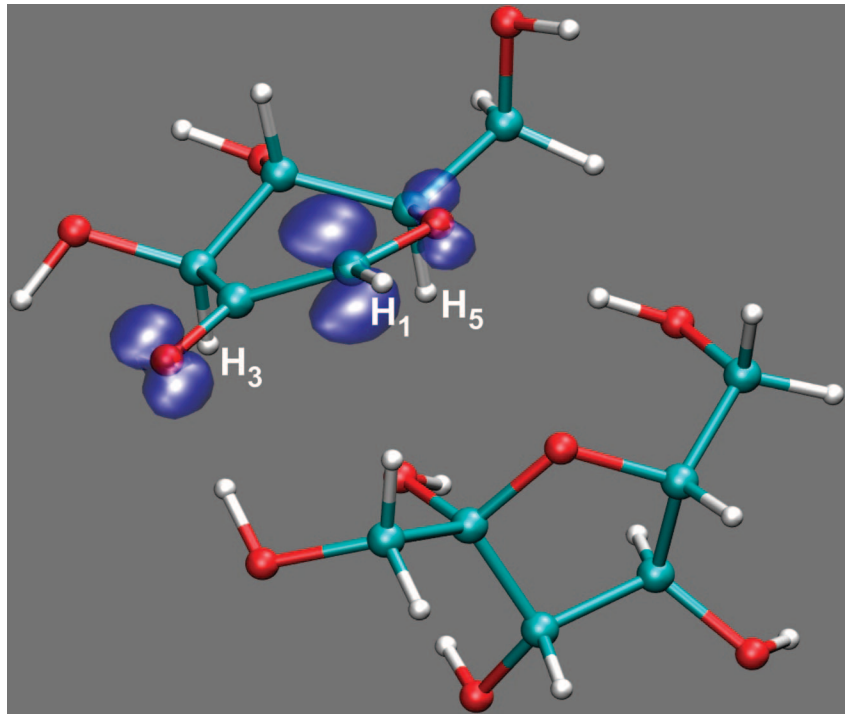

Figure 4. Optimized structure of radical model M_1. The spin density distribution is visualized by means of a spin density isosurface with $\rho = 0.04$ (blue).

TABLE 4: Proton Hyperfine Coupling Tensors (in MHz) for Radical Model M_1, Obtained by Means of DFT Calculations in a <2a2b2c> Supercell[a]

				eigenvectors				δ (°)	
radical model	proton	iso	aniso	a*	b	c	proton	T2	T3
$\mathbf{M_1}$	$\mathbf{H_1}$	−35.22	−20.46	−0.441	0.164	0.882	$\mathbf{H_\alpha}$	1.2	9.8
			−4.64	0.889	0.215	0.405		4.2	17.3
			25.10	−0.123	0.963	−0.241		4.1	15.6
	$\mathbf{H_3}$	16.17	−2.17	0.905	0.416	0.091	$\mathbf{H_{\beta 1}}$	25.5	10.8
			−1.84	−0.182	0.184	0.966		25.2	8.9
			4.02	−0.385	0.891	−0.242		4.0	12.6
	$\mathbf{H_5}$	12.60	−2.85	0.733	0.610	0.302	$\mathbf{H_{\beta 2}}$	4.0	17.7
			−2.06	0.650	−0.497	−0.576		2.4	13.0
			4.91	0.201	−0.618	0.760		4.6	14.6

[a] The deviation δ between the calculated eigenvectors and the eigenvectors of T2 and T3 (Table 1) are given in the right-hand columns.

calculated parameters and the experimental data for T2 is striking. The eigenvectors are in remarkably good accordance, especially for the H_α HF coupling. The eigenvectors associated with $b_{+,\mathrm{dip}}$ differ in direction by no more than 2.5° for all three tensors. The match in anisotropic values is excellent. Some minor discrepancies are encountered for the isotropic coupling values, in particular, for the H_α HF coupling, but these values are known to be much more sensitive to basis set effects and the level of theory.[51] In conclusion, the overall agreement found between calculated and experimentally determined data strongly suggests that M_1 essentially is the correct model for the T2 radical in RT X-irradiated sucrose single crystals.

The optimized geometry of model M_1 is shown in Figure 4. The C_1 and C_2 centers attain a close-to-planar configuration and the glucose and fructose units have slightly shifted away from each other, obtaining stable configurations by way of the hydrogen bonds with the neighboring molecules. Figure 4 clearly shows that the unpaired spin density is localized not only on C_1 and the carbonyl oxygen but also on the ring oxygen. Furthermore, protons H_3 and H_5 are oriented roughly parallel with the LEO axes. These two observations explain why both of the γ-proton couplings exhibit substantial isotropic components.

As the agreement between M_1 and T3 is also quite good (Table 3), one could also associate M_1 to T3. The differences in isotropic and anisotropic values between radicals T2 and T3 are indeed very small, but the eigenvector directions appear to provide a sufficient criterion for discriminating between them. Most strikingly, the eigenvectors associated with $b_{+,\mathrm{dip}}$ all deviate more than 10° from the experimental ones for the T3 radical (Table 3). To assess the credibility of the calculated parameters in this context, the dependency of the calculated EMR parameters on the supercell size was investigated. A geometry optimization was performed in a <2a2b2c> supercell, and EMR parameters were calculated in the same cluster approach employed above. The results are shown in Table 4. The agreement with the experimental data of T2 is still striking, but more importantly, the differences between the results of the two different supercell calculations are considerably smaller than the differences in experimental parameters for T2 and T3. Therefore, it appears to be meaningful to state that radical model M_1 corresponds to T2 and not to T3.

TABLE 5: Experimentally Determined g Tensor for Radical R1 at Room Temperature[16] and Calculated g Tensors for Conformations A and B of Radical Model M_1, Obtained As Described in the Computational Procedures Section[a]

				eigenvectors			
			principal values	a*	b	c	δ (°)
experiment	R1[b]		2.0027	−0.882	0.187	−0.435	
			2.0049	0.022	−0.902	−0.432	
			2.0067	−0.472	−0.391	0.790	
calculations	conformation A	Approach #1	2.0021	−0.642	−0.208	−0.738	32.0
			2.0060	0.253	−0.966	0.052	31.3
			2.0076	−0.724	−0.153	0.673	21.1
		Approach #2	2.0022	−0.807	−0.192	−0.558	23.2
			2.0063	0.429	−0.841	−0.331	24.4
			2.0079	−0.406	−0.506	0.761	7.9
	conformation B	Approach #1	2.0022	−0.644	−0.194	−0.740	31.4
			2.0061	0.244	−0.969	0.042	30.5
			2.0073	−0.725	−0.154	0.672	21.1
		Approach #2	2.0020	−0.768	−0.164	−0.619	23.7
			2.0071	0.329	−0.931	−0.161	23.6
			2.0098	−0.549	−0.327	0.769	6.0

[a] The deviation δ between the calculated eigenvectors and the eigenvectors of R1 are given in the right-hand columns. [b] Reference 16.

Next to HF parameters, g tensors were also calculated for Approach #1, using the two models discussed in Computational Procedures. Sagstuen and co-workers determined the g tensor for one of the stable radicals (labeled R1) in sucrose single crystals from Q-band EPR angular variations at RT.[16] It was shown in our previous paper[20] that the R1 radical corresponds to the T3 radical in the current work (Table 1). In Table 5, the results of the g tensor calculations are given and compared to the experimental data. Concerning the latter, some corrections have been applied, after consulting the authors concerned. The calculated principal values are similar between the two models and in reasonable qualitative agreement with the experimental data. The eigenvectors obtained in Approach #2 are substantially better in accordance with the experimental eigenvectors than those obtained in Approach #1. This can be ascribed to the fact that in Approach #2, the radical environment is taken into account. It was concluded above that model M_1 corresponds to radical T2, whereas the g tensor determined experimentally is associated with radical T3. This probably accounts for part of the discrepancy between the calculations and the experimental data. No further conclusions can be drawn until more experimental data, the g tensor of the T2 radical in particular, are available.

Finally, another model closely related to M_1 was investigated. Labeled M_6 and depicted in Figure 3, it is a simple alternative to M_1 where all key features are maintained: the presence of the α proton, a neighboring carbonyl group, and two γ protons. This structure presumes a glucose ring rupture and not a glycosidic bond cleavage. However, the optimized geometry differs drastically from that of M_1, and consequently, the calculated HF parameters differ substantially from the experimental values (see Table 3). This supports the suggestion that the chemical structure of radical T2 is properly described by model M_1. Furthermore, it indicates that the T3 radical most likely differs from T2 by more subtle changes in conformation, for example, because of differences in the conformation of the environment. This point is further addressed in the next section.

3.3. In Search for T3: A Conformational Study of Radical Model M_1. The simultaneous presence of several quite similar radiation-induced radicals has previously been reported for a number of sugar derivatives, for example, sucrose,[18,20] fructose,[10] and sorbose.[52] Possible reasons have been explored in literature: for fructose in terms of temperature effects[29] and for sorbose in terms of the naturally present disorder in the pristine lattice.[53] Neither of the studies was able to provide an explanation, however. Therefore, it must be assumed that radiation, starting from the same pristine molecule, somehow gives rise to several distinguishable but structurally very similar radical species. As the calculations above indicate that the radicals most likely do not differ from each other in chemical structure, one might explore the two possible scenarios below. Evidently, an exhaustive exploration of these possibilities would be very time-consuming and is beyond the scope of the present paper. Therefore, a small set of alternative conformations was selected, in order to obtain a rough idea of the sensitivity of the hyperfine tensors on the radical conformation.

Scenario 1: The Similar Radicals Are Chemically Identical but Correspond to Different Local Minima on the Potential Energy Surface (PES). Comparison of the radical structure with the pristine crystal structure reveals that for two hydroxy groups, in particular, other orientations (than those in M_1) could give rise to alternative minima in the PES: the $O_{2'}-H(O_{2'})$ hydroxy group at the $C_{2'}-$carbon of the fructose unit and the $O_{6'}-H(O_{6'})$ hydroxy group at the fructose $C_{6'}-$carbon of a neighboring molecule. In the pristine lattice structure, the latter hydroxy group is connected through an intermolecular hydrogen bond to the $H(O_2)$ hydroxy hydrogen. (Figure 5A,B).

In order to investigate this, rotational scans of both hydroxy groups were performed where the proper dihedral angles $H(O_{2'})-O_{2'}-C_{2'}-C_{3'}$ (D_1) and $H(O_{6'})-O_{6'}-C_{6'}-C_{5'}$ (D_2) (cf. Figure 5C,D, respectively) were varied over 360° in 15° steps. For each value of the dihedral angle, an optimization was performed for which the dihedral angle was constrained. The energy profile for the rotational scan of the $O_{2'}-H(O_{2'})$ group is shown in Figure 6A and reveals two local minima ($D_1 \approx 90°$ and $D_1 \approx 330°$). Starting from the radical structures associated with each of these minima, a nonconstrained optimization was performed, and the corresponding points are marked in Figure 6A as points B and A, respectively. Conformer A ($D_1 = 329.7°$, Figure 5B) is the most stable and corresponds to model M_1 as discussed above. Conformer B ($D_1 = 98.6°$, Figure 5C) is about 9.2 kJ/mol ($\approx$ 95 meV) higher in energy. The configuration of the glucose ring containing the radical site is virtually identical in the two conformers. The energy profile indicates that conformer B is unlikely to account for the T3 radical. Also, Tables 5 and 6 show that the differences between the calculated

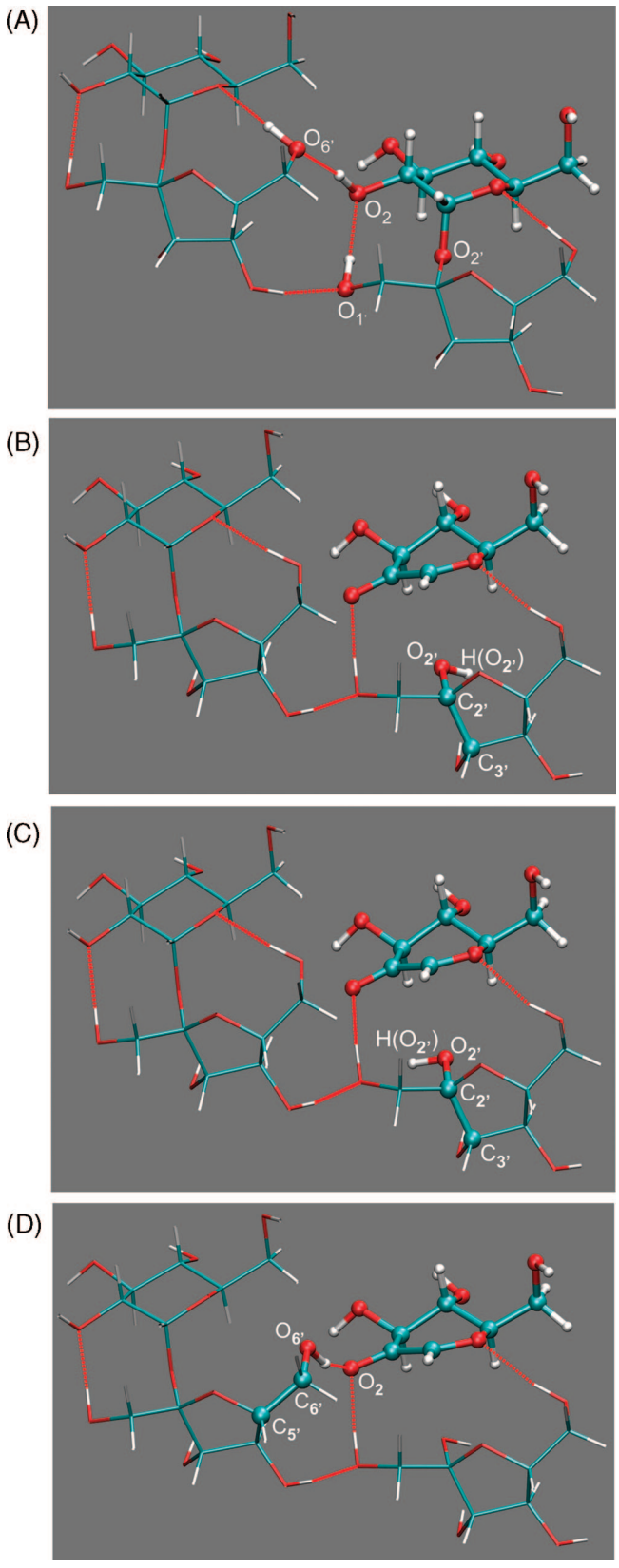

Figure 5. Conformation of the radical molecule and a neighboring molecule in the pristine lattice (A) and in the alternative local minima A, B, and C of model M_1 (B, C, and D, respectively; cf. Figure 6).

EMR parameters for the two conformers are very small and negligible as compared with the differences between T2 and T3.

The energy profile for the rotational scan of the $O_{6'}-H(O_{6'})$ hydroxy group is shown in Figure 6B. Again, two local minima

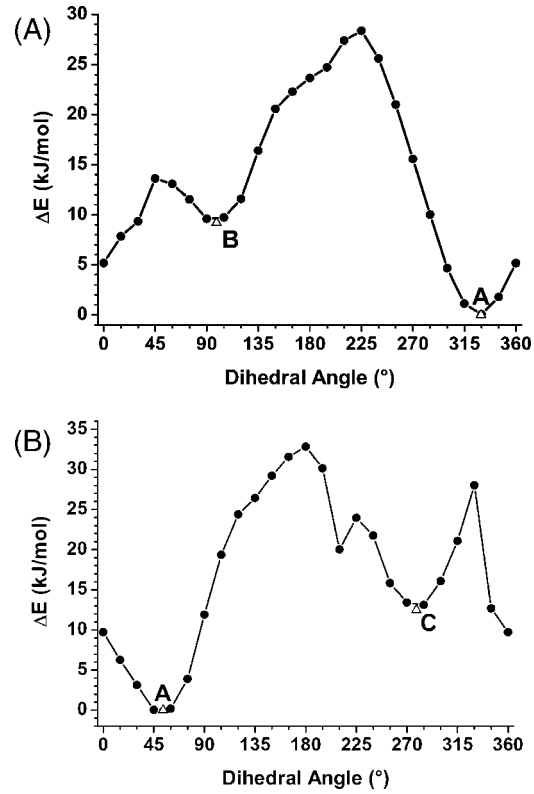

Figure 6. (A) Energy profile for the rotation of the $O_{2'}-H_{2'}$ hydroxy group about the $O_{2'}-C_{2'}$ bond in model M_1. (B) Energy profile for the rotation of the $O_{6'}-H(O_{6'})$ hydroxy group about the $O_{6'}-C_{6'}$ bond of the neighboring molecule (Figure 5) in model M_1. The round points indicate the results of constrained optimizations, the triangles those of nonconstrained optimizations. Conformer A has the lowest energy ($E = -2.708866 \times 10^6$ kJ/mol) and was taken as a reference.

are present with the deepest minimum corresponding to conformer A ($D_2 = 53.3°$). Conformer C ($D_2 = 278.5°$) is depicted in Figure 5D. Reorganization of the hydrogen bonds results in a slightly different configuration of the glucose ring where the unpaired spin is residing. Both the energy profile of Figure 6B and the EMR parameters calculated for conformer C (Table 6) again dismiss it as a candidate for T3.

Scenario 2: Immediate Environments of the Similar Radicals Differ in Chemical Structure. In model M_7 (Figure 3), a formaldehyde molecule is split off from the $C_{2'}$ carbon of the fructose unit, implying that two additional hydrogens are removed as compared with model M_1. Thus, the intramolecular $O_2-H(O_{1'})$ hydrogen bond (Figure 5A), which constitutes the most direct link from the fructose unit to the glucose unit for model M_1, is broken. This model may serve as a tool to probe the sensitivity of the calculated HF tensors to changes in the fructose ring. With regard to the radical center, the optimized geometry differs from M_1 mainly in that the C_2 center becomes substantially more planar. The results given in Table 3 show that this gives rise to relatively small but noticeable differences in the calculated tensors. The overall agreement with the experimental results is, however, worse. But more important from a general point of view, the calculated eigenvectors corresponding to $b_{+,\mathrm{dip}}$ of all three couplings are only rotated by a few degrees as compared with those of M_1.

These results show that relatively subtle differences in conformation can easily lead to substantial changes in the isotropic coupling values, especially those of the γ-proton couplings, as well as in the direction of the eigenvectors associated with the intermediate and smallest anisotropic

TABLE 6: Calculated Proton Hyperfine Coupling Tensors (in MHz) for Conformations A, B, and C of Model M_1, Corresponding to Local Minima in the Energy Profiles of Figure 6, and Depicted in Figure 5B,C,D, respectively[a]

				Eigenvectors				δ (°)	
conformation	proton	iso	aniso	a*	b	c	proton	T2	T3
A	$\mathbf{H_1}$	−34.60	−20.23	−0.451	0.155	0.879	$\mathbf{H_\alpha}$	1.8	9.3
			−4.66	0.875	0.267	0.403		2.1	14.3
			24.89	−0.173	0.951	−0.256		1.2	13.0
	$\mathbf{H_3}$	16.18	−2.16	0.874	0.462	0.154	$\mathbf{H_{\beta 1}}$	29.5	11.9
			−1.86	−0.249	0.152	0.957		29.5	11.4
			4.02	−0.418	0.874	−0.248		1.9	10.9
	$\mathbf{H_5}$	12.59	−2.88	0.675	0.673	0.303	$\mathbf{H_{\beta 2}}$	4.2	13.1
			−2.06	0.698	−0.450	−0.557		4.7	9.5
			4.95	0.239	−0.588	0.773		2.5	12.2
B	$\mathbf{H_1}$	−32.30	−18.82	−0.446	0.146	0.883	$\mathbf{H_\alpha}$	1.6	9.8
			−4.77	0.875	0.281	0.395		1.5	13.7
			23.59	−0.191	0.948	−0.253		0.3	12.5
	$\mathbf{H_3}$	18.86	−2.13	0.907	0.403	−0.125	$\mathbf{H_{\beta 1}}$	13.0	10.3
			−1.94	0.004	0.289	0.957		13.0	10.9
			4.07	−0.422	0.868	−0.261		1.8	10.1
	$\mathbf{H_5}$	12.75	−2.85	0.643	0.699	0.314	$\mathbf{H_{\beta 2}}$	6.4	11.3
			−2.03	0.725	−0.423	−0.544		6.9	7.6
			4.88	0.247	−0.577	0.778		2.5	11.5
C	$\mathbf{H_1}$	−34.25	−19.44	−0.412	0.125	0.903	$\mathbf{H_\alpha}$	2.3	12.3
			−4.80	0.893	0.254	0.372		1.6	15.8
			24.23	−0.183	0.959	−0.216		2.8	14.7
	$\mathbf{H_3}$	18.42	−2.28	0.889	0.440	−0.127	$\mathbf{H_{\beta 1}}$	13.5	8.4
			−1.91	0.009	0.261	0.965		13.4	11.7
			4.20	−0.458	0.859	−0.228		1.2	10.4
	$\mathbf{H_5}$	13.61	−2.77	0.664	0.681	0.310	$\mathbf{H_{\beta 2}}$	5.0	12.6
			−2.06	0.700	−0.420	−0.578		5.0	10.0
			4.83	0.263	−0.601	0.755		0.8	13.2

[a] The tensors were obtained as described in the Computational Procedures section. The deviation δ between the calculated eigenvectors and the eigenvectors of T2 and T3 (Table 1) are given in the right-hand columns.

coupling values. The anisotropic coupling constants and the direction of the eigenvector associated with $b_{+,\mathrm{dip}}$ are less dependent on the exact conformation of the radical environment. The differences between T2 and T3, however, are rather opposite: very similar in isotropic and anisotropic coupling values but differing in eigenvector directions. It is tentatively concluded that T2 and T3 do not differ in chemical structure but that the differences in conformation, either of the radical or of its surrounding between T2 and T3, must be rather substantial to account for the differences in eigenvector directions.

EPR, ENDOR, and EIE measurements after in situ 10 K X-irradiation of sucrose single crystals together with corresponding DFT calculations are currently being made in our laboratories in order to determine the precursors and the formation mechanisms of the sucrose radicals stable at RT. This hopefully will give insight into the exact structure of the T3 radical and explain its presence. The results of these investigations will be the subject of a forthcoming publication.

4. Conclusions

Radical T2, one of the major stable radiation-induced radicals in sucrose single crystals, has been identified by means of DFT calculations as a C_1 centered radical. The radical structure involves scission of the glycosidic bond linkage at the glucose side and the presence of a carbonyl group at the C_2 position. The agreement between calculated and experimentally observed EMR parameters is excellent on all accounts. A limited conformational study of this radical model indicates that radical T3 is very likely chemically identical to T2 and that alternative orientations of neighboring hydroxy groups or alternative configurations of the neighboring fructose ring do not offer an explanation for the presence or characteristics of T3.

Acknowledgment. The authors H.D.C., E.P., and H.V. wish to thank the Fund for Scientific Research−Flanders for financial support.

References and Notes

(1) Samskog, P. O.; Lund, A.; Nilsson, G.; Symons, M. C. R. *J. Chem. Phys.* **1980**, *73*, 4862–4866.
(2) Samskog, P. O.; Lund, A. *Chem. Phys. Lett.* **1980**, *75*, 525–527.
(3) Samskog, P. O.; Kispert, L. D.; Lund, A. *J. Chem. Phys.* **1983**, *79*, 635–638.
(4) Budzinski, E. E.; Box, H. C. *J. Chem. Phys.* **1985**, *82*, 3487–3490.
(5) Box, H. C.; Budzinski, E. E.; Freund, H. G. *Radiat. Res.* **1990**, *121*, 262–266.
(6) Sagstuen, E.; Lindgren, M.; Lund, A. *Radiat. Res.* **1991**, *128*, 235–242.
(7) Bungum, B.; Hole, E. O.; Sagstuen, E.; Lindgren, M. *Radiat. Res.* **1994**, *139*, 194–202.
(8) Madden, K. P.; Bernhard, W. A. *J. Phys. Chem.* **1980**, *84*, 1712–1717.
(9) Madden, K. P.; Bernhard, W. A. *J. Phys. Chem.* **1982**, *86*, 4033–4036.
(10) Vanhaelewyn, G.; Lahorte, P.; De Proft, F.; Mondelaers, W.; Geerlings, P.; Callens, F. *Phys. Chem. Chem. Phys.* **2001**, *3*, 1709–1716.
(11) Samskog, P.-O.; Kispert, L. D.; Lund, A. *J. Chem. Phys.* **1983**, *78*, 5790–5794.
(12) Samskog, P.-O.; Kispert, L. D.; Lund, A. *J. Chem. Phys.* **1982**, *77*, 2330–2335.
(13) Gräslund, A.; Löfroth, G. *Acta Chem. Scand. B* **1975**, *29*, 475–482.
(14) Budzinski, E. E.; Potter, W. R.; Potienko, G.; Box, H. C. *J. Chem. Phys.* **1979**, *70*, 5040–5044.
(15) Box, H. C.; Budzinski, E. E. *J. Chem. Phys.* **1983**, *79*, 4142–4145.
(16) Sagstuen, E.; Lund, A.; Awaldelkartim, O.; Lindgren, M.; Westerling, J. *J. Chem. Phys.* **1986**, *90*, 5584–5588.
(17) Box, H. C.; Budzinski, E. E.; Freund, H. G. *J. Chem. Phys.* **1990**, *93*, 55–57.
(18) Vanhaelewyn, G.; Sadlo, J.; Callens, F.; Mondelaers, W.; De Frenne, D.; Matthys, P. *Appl. Radiat. Isot.* **2000**, *52*, 1221–1227.

(19) Georgieva, E. R.; Pardi, L.; Jeschke, G.; Gatteschi, D.; Sorace, L.; Yordanov, N. D. *Free Radical Research* **2006**, *40*, 553–563.
(20) De Cooman, H.; Pauwels, E.; Vrielinck, H.; Dimitrova, A.; Yordanov, N.,; Sagstuen, E.; Waroquier, M.; Callens, F. *Spectrochim. Acta A* **2008**, *69*, 1372–1383.
(21) McConnell, H. M.; Chesnut, D. B. *J. Chem. Phys.* **1958**, *28*, 107–117.
(22) Heller, C.; McConnell, H. M. *J. Chem. Phys.* **1960**, *32*, 1535.
(23) Øhman, K. T.; Sanderud, A.; Hole, E. O.; Sagstuen, E. *J. Phys. Chem. A* **2006**, *110*, 9585–9596.
(24) Vanhaelewyn, G.; Pauwels, E.; Callens, F.; Waroquier, M.; Sagstuen, E.; Matthys, P. *J. Phys. Chem. A* **2006**, *110*, 2147–2156.
(25) Pauwels, E.; Van Speybroeck, V.; Waroquier, M. *J. Phys. Chem. A* **2006**, *110*, 6504–6513.
(26) Jayatilaka, N.; Nelson, W. H. *J. Phys Chem. B* **2007**, *111*, 800–810.
(27) Jayatilaka, N.; Nelson, W. H. *J. Phys. Chem. B* **2007**, *111*, 7887–7896.
(28) Pauwels, E.; Declerck, R.; Van Speybroeck, V.; Waroquier, M. *Radiation Research* **2008**, *169*, 8–18.
(29) Declerck, R.; Pauwels, E.; Van Speybroeck, V.; Waroquier, M. *J. Phys. Chem. B*, **2008**, *112*, 1508–1514.
(30) CPMD V3.11, Copyright IBM Corp., 1990−2006, Copyright MPI fuer Festkoerperforschung, Stuttgart, 1997−2001.
(31) Perdew, J. P. *Phys. Rev. B* **1986**, *33*, 8822–8824.
(32) Becke, A. D. *J. Chem. Phys.* **1992**, *96*, 2155–2160.
(33) Vanderbilt, D. *Phys. Rev. B* **1990**, *41*, 7892–7895.
(34) Declerck, R.; Pauwels, E.; Van Speybroeck, V.; Waroquier, M. *Phys. Rev. B* **2006**, *74*, 245103.
(35) Pauwels, E.; Van Speybroeck, V.; Waroquier, M. *Spectrochimica Acta Part A* **2006**, *63*, 795–801.
(36) Frisch, M. J. Trucks G. W., Schlegel H. B., Scuseria, G. E. Robb, M. A. Cheesemam, J. R. Montgomery, J. J. A. Vreven, T. N. Kudin, K. Burant, J. C. Millam, J. M. Lyengar, S. S. Tomasi, J. Barone, V. Mennucci, B. Cossi, M. Scalmani, G. Rega, N. Petersson, G. A. Nakatsuji, H. Hada, M. Ehara, M. Toyota, K. Fukuda, R. Hasegawa, J. Ishida, M. Nakajima, T. Honda, Y. Kitao, O. Nakai, H. Klene, M. Li, X. Knox, J. E. Hratchian, H. P. Cross, J. B. Adamo, C. Jaramillo, J. Gomperts, R. Stratmann, R. E. Yazyev, O. Austin, A. J. Cammi, R. Pomelli, C. Ochterski, J. W. Ayala, P. Y. Morokuma, K. Voth, G. A. Salvador, P. Dannenberg, J. J. Zakrzewski, V. G. Dapprich, S. Daniels,A. D. Strain, M. C. Farkas, O. Malick, D. K. Rabuck, A. D. Raghavachari, K. Foresman, J. B. Ortiz, J. V. Cui, Q. Baboul, A. G. Clifford, S. Cioslowski, J. Stefanov, B. B. Liu, G. Liashenko, A. Piskorz, P. Komaromi, I. Martin, R. L. Fox, D. J. Keith, T. Al-Laham, M. A. Peng, C. Y. Nanayakkara, A. Challacombe, M. Gill, P. M. W. Johnson, B. Chen, W. Wong, M. W. Gonzalez, C. Pople, J. A. Gaussian 03, Revision B.03, Gaussian, Inc.: Pittsburgh, PA, 2003.
(37) Becke, A. D. *J. Chem. Phys.* **1996**, *104*, 1040–1046.
(38) Krishnan, R.; Binkley, J. S.; Seeger, R.; Pople, J. A. *J. Chem. Phys.* **1980**, *72*, 650–654.
(39) McLean, A. D.; Chandler, G. S. *J. Chem. Phys.* **1980**, *72*, 5639–5648.
(40) Declerck, R.; Van Speybroeck, V.; Waroquier, M. *Phys. Rev. B* **2006**, *73*, 115113.
(41) Becke, A. D. *Phys. Rev. A* **1988**, *38*, 3098.
(42) Lee, C.; Yang, W.; Parr, R. G. *Phys. Rev. B* **1988**, *37*, 785.
(43) Goedecker, S.; Teter, M.; Hutter, J. *J. Phys. Rev. B* **1996**, *54*, 1703.
(44) Erling, P. A.; Nelson, W. H. *J. Phys. Chem. A* **2004**, *108*, 7591–7595.
(45) Bernhard, W. A. *Adv. Radiat. Biol.* **1981**, *9*, 199.
(46) Bernhard, W. A. *J. Chem. Phys.* **1984**, *81*, 5928–5935.
(47) Flores, J.; Cabrera, B. E.; Calderon, T.; Muñoz, P. E.; Adem, E.; Hernandez, J.; Boldu, B. L.; Murrieta, H. *Appl. Radiat. Isot.* **2000**, *52*, 1229–1234.
(48) Yordanov, N. D.; Karakirova, Y. *Radiation Measurements*, in press, doi:10.1016/j.radmeas. 2006.10.004.
(49) Box, H. C.; Budzinski, E. E.; Potienko, G. *J. Chem. Phys.* **1980**, *73*, 2052–2056.
(50) Brown, G. M.; Levy, H. A. *Acta Crystallogr., Sect. B: Struct. Crystallogr. Cryst. Chem.* **1973**, *29*, 790–797.
(51) Improta, R.; Barone, V. *Chem. Rev.* **2004**, *104*, 1231–1253.
(52) Jansen, B. *Radiation Induced Radicals in Single Crystals of* α*-L-sorbose. ESR-, ENDOR- and pulse radiolysis studies at room temperature,* Master Thesis, University of Oslo, 1992; in Norwegian.
(53) Vanhaelewyn, G. C. A. M.; Jansen, B.; Pauwels, E.; Sagstuen, E.; Waroquier, M.; Callens, F. J. *J. Phys. Chem. A* **2004**, *108*, 3308–3314.

JP712004G